PUBLISHED BY IOP PUBLISHING FOR SISSA MEDIALAB
RECEIVED: *November 18, 2012*
ACCEPTED: *February 12, 2013*
PUBLISHED: *March 13, 2013*

A pixel detector system for laser-accelerated ion detection

S. Reinhardt,[a,1] **W. Draxinger,**[a] **J. Schreiber**[a,b] **and W. Assmann**[a]

[a]*Fakultät für Physik, Ludwig-Maximilians-Universität München, Am Coulombwall 1, 85748 Garching, Germany*
[b]*Max-Planck-Institut für Quantenoptik, Hans-Kopfermann-Str. 1, 85748 Garching, Germany*

E-mail: Sabine.Reinhardt@physik.uni-muenchen.de

ABSTRACT: Laser ion acceleration is an unique acceleration process that creates ultra-short ion pulses of high intensity ($> 10^7$ ions/cm^2/ns), which makes online detection an ambitious task. Non-electronic detectors such as radio-chromic films (RCF), imaging plates (IP) or nuclear track detectors (e.g. CR39) are broadly used at present. Only offline information on ion pulse intensity and position are available by these detectors, as minutes to hours of processing time are required after their exposure. With increasing pulse repetition rate of the laser system, there is a growing need for detection of laser accelerated ions in real-time.

Therefore, we have investigated a commercial pixel detector system for online detection of laser-accelerated proton pulses. The CMOS imager RadEye1 was chosen, which is based on a photodiode array, 512×1024 pixels with 48 μm pixel pitch, thus offering a large sensitive area of approximately 25×50 mm^2. First detection tests were accomplished at the conventional electrostatic 14 MV Tandem accelerator in Munich as well as Atlas laser accelerator. Detector response measurements at the conventional accelerator have been accomplished in a proton beam in dc (15 MeV) and pulsed (20 MeV) irradiation mode, the latter providing comparable particle flux as under laser acceleration conditions. Radiation hardness of the device was studied using protons (20 MeV) and C-ions (77 MeV), additionally. The detector system shows a linear response up to a maximum pulse flux of about 10^7 protons/cm^2/ns. Single particle detection is possible in a low flux beam (10^4 protons/cm^2/s) for all investigated energies. The radiation hardness has shown to give reasonable lifetime for an application at the laser accelerator. The results from the irradiation at a conventional accelerator are confirmed by a cross-calibration with CR39 in a laser-accelerated proton beam at the MPQ Atlas Laser in Garching, showing no problems of detector operation in presence of electro-magnetic pulse (EMP). The calibrated detector system was finally used for online detection of laser-accelerated proton and carbon ions at the Astra-Gemini laser.

KEYWORDS: Solid state detectors; Instrumentation for particle accelerators and storage rings - low energy (linear accelerators, cyclotrons, electrostatic accelerators); Instrumentation for heavy-ion accelerators

[1]Corresponding author.

doi:10.1088/1748-0221/8/03/P03008

Contents

2013 JINST 8 P03008

1 Introduction

Laser-driven acceleration of ions and electrons offers the potential to build compact accelerators in the future [1]. Typically used TW laser systems have intensities exceeding 10^{18} W/cm^2 and pulse durations ranging from few tens of femtoseconds to picoseconds. The interaction of such a highly intense short laser pulse with a thin target foil (nm to μm thickness depending on the condition) generates a charge-separation field at the foil boundaries with magnitudes beyond TV/m. In such high fields, atoms are ionized and effectively accelerated to MeV energies over few micrometer distances [2, 3].

Laser accelerated ion beams have due to the unique acceleration process very special properties. In particular, they are created in ultra-short particle pulses of high intensity ($> 10^7$ particles/cm^2/ns), which makes online detection difficult. Saturation problems due to the peculiar time structure and intensity of these pulses, are likely for usual electronic detectors, that are optimized for statistical particle rates up to 100 kHz. Generation of an electro-magnetic pulse (EMP) during laser-target interaction can cause additional problems for electronic devices.

Non-electronic devices such as Image Plates (IP), radiochromic films (RCF) or nuclear track detectors (e.g CR39) are therefore still state of the art in detection of laser-accelerated particle beams [4–8]. To obtain quantitative results from these detectors, processing times of several hours

to days are typical. Furthermore, the majority of these devices allow only single use. They can apparently not be used with few Hz repetition rate laser systems, becoming more and more available. As a result, ion diagnostic for laser accelerators is in an urgent need for online detection systems.

Energy spectra of laser-accelerated ions typically show up to 100% energy spread depending on the acceleration regime. Ion detection usually takes place behind an energy spectrometer, with IP or CR39 applied as sensitive element [4, 5, 8]. Some groups started to replace these detectors by micro-channel plates (MCP) [9–12]. MCPs, initially designed for electron multiplication, can also be used as space-resolved detector. For this purpose, the MCPs amplified electron signal is detected by a phosphor screen and the scintillation light observed by a CCD-camera. With respect to laser-plasma experiments, high vacuum demands ($< 10^{-6}$ mbar) because of the required high voltage for MCP operation adds a further step on complexity to the experimental setup of such a MCP-based system. We decided to follow an alternative approach and investigated a semiconductor pixel detector for real time detection of laser accelerated ions [13]. The availability of many different pixel detector architectures with sub-mm pixel pitch as well as ease of use make them interesting candidates for simple space-resolved detector systems. As each pixel represents a small detector unit in itself, only a small fraction of the whole ion pulse will be detected by each pixel. Hence, problems due to detector saturation might be overcome by this approach.

For detection tests we chose a commercial system, based on a CMOS photodiode array, the RadEye 1 sensor (Teledyne Rad-icon Imaging Corporation). The detector response to single protons as well as intense proton pulses was studied at an electrostatic Tandem accelerator as well as a laser accelerator for different proton energies. The radiation hardness of the device was investigated using protons and C-ions at a conventional accelerator, only. As MCPs are used at the laser accelerator similarly to the investigated pixel detector system, results of the measurements are discussed particularly in comparison with typical MCP characteristics.

2 Material and methods

2.1 Detector system

The RadEye sensor is designed for digital radiography applications such as mammography or industrial inspection [14–16]. A scintillator screen, converting incident X-rays into visible light, is usually directly coupled to the sensor for this kind of applications [15]. The thickness of the depletion zone and passivation layer, respectively, are, thus, in the order of few μm.

The CMOS imager has a matrix of 512×1024 pixels with 48 μm pixel pitch, offering a large sensitive area of 24.6 mm by 49.2 mm. Tiling of additional sensor modules is possible at three sides of the detector, allowing a further increase of the sensitive area with a dead gap in between two sensors of only 100 μm.

The quoted typical saturation limit per pixel of 2.8×10^6 electrons corresponds to a maximum fluence of 20 MeV protons of approximately $10^7/\text{cm}^2$. Data acquisition (DAQ) was based on the Remote RadEye Camera System with Ethernet interface, which allows parallel read-out of up to 4 sensors. To synchronize the detector read-out with the laser (ion) pulse the system was adapted to our specific needs with a custom made trigger control unit and in-house written software tool. Different detector grades are available from the manufacturer, for our purpose engineering grade detectors with up to 10% defective pixel were sufficient for irradiation experiments [15].

2013 JINST 8 P03008

2.2 Experimental setup

2.2.1 Munich Tandem accelerator

First detector tests of the detector system were accomplished at the Munich Tandem accelerator, a conventional electrostatic accelerator [13]. Irradiation in continuous as well as pulsed beam mode is possible, the latter allowing preparation of ns-pulses with a maximum flux of 10^7 particles/cm^2/ns when using a brilliant multicusp ion source [17], which are, hence, comparable to laser-accelerated proton pulses. The range of available proton energies of up to 25 MeV covers the energy range currently available by laser acceleration at the Atlas laser of the Max-Planck-Institute for Quantum optics (MPQ) in Garching.

Radiation damage investigations have been accomplished in a 20 MeV proton beam as well as with 77 MeV C-ions. All measurements with protons have been accomplished in air, using a circular Kapton exit window of 10 mm diameter and 50 μm thickness. Radiation hardness was studied up to a maximum proton fluence of $6 \cdot 10^{10}$ protons/cm^2, which was determined by a calibrated Faraday Cup (FC). In addition, the detector response in pre-damaged areas was studied in pulsed beam mode up to a maximum flux of 10^5p/cm^2/ns.

For carbon damage studies, the sensor was mounted in vacuum and irradiated with 77 MeV C-ions to six fluence levels between 10^7 and 10^{12} particles/cm^2. Measurements of the dark pixel value were accomplished in air before and after these irradiations.

2.2.2 MPQ Atlas laser

A cross-calibration measurement with CR39 in a laser-accelerated proton beam was carried out at the Atlas laser. Atlas is a Ti:Sapphire laser system, operated at a wavelength of 795 nm with maximal pulse repetition rate of 10 Hz. In these experiments peak pulse energy of 0.4 J is delivered within a 30 fs pulse (FWHM). Diamond like carbon (DLC) foils of 5–40 nm thickness were used as target [19]. The diameter (FWHM) of the laser spot, focused onto the target by an off-axis parabolic mirror, was approximately 3 μm.

The detector was mounted in vacuum behind a magnetic spectrometer. To measure an angular-resolved energy spectrum, a slit of 14 cm length and 300 μm width, oriented parallel to the vertical magnetic field lines, is used as entrance of the spectrometer. Dipole magnet with 100–200 mT over 20 cm length is used (i.e. Wien filter).

Protons and C-ions are simultaneously accelerated by the laser-plasma interaction. To filter all contributions of C-ions from the proton spectrum an Al foil of 11 μm thickness was placed in front of the detector, shielding all ambient light from the light-sensitive detection area as well. Only protons with energies exceeding about 1 MeV were detected in the sensitive detector layer due to the Al filter.

Four sensor modules tiled at their longer side were mounted. One half of the total sensitive detector area of 100×50 mm^2 was covered by 1 mm thick plates of CR39. Only protons with energies below 4 MeV create tracks on CR39, that are visible under a microscope after etching [8]. Ions with broad spectra up to maximum proton energies of about 3 MeV, thus allowed direct detection on CR39.

CR39 plates were etched for 90 minutes at a temperature of 80°C in a six-molar caustic soda solution few days after exposure to prevent track fading. Etched plates were analyzed by an au-

2013 JINST 8 P03008

tomatic track counting microscope system, similar to the system presented in refs. [19, 20]. An appropriate background correction was applied to all pixel detector data before analysis.

2.2.3 Astra Gemini laser

The calibrated detector system was used as online diagnostic for proton and carbon ion detection at the Astra Gemini Laser of the Rutherford Appleton Laboratory (RAL). The laser delivers 4–6 J pulse energy to the target in a pulse of 50 fs duration at a wavelength of 800 nm. The laser was focused to 3 μm (FWHM) on the target, a 75 nm thin plastic foil. The setup contained an electromagnetic spectrometer to separate individual ion species according to their charge-to-mass ratio. The solid angle is defined by a set of vertical and horizontal slits with 160 μm and 100 μm width, respectively. As light shield, 15 μm thick Al foil was used, blocking all proton (carbon ion) contributions with energies below 1.1 MeV (20 MeV). However, in case of the proton spectrum the lower cut-off energy of about 4 MeV was defined by geometrical constraints.

3 Results

3.1 Detector response

Detector response to single protons as well as intense ion pulses (up to 10^6 protons/cm^2) was studied in a continuous 15 MeV and pulsed 20 MeV proton beam, respectively. No charge sharing effects between neighbour pixels (blooming), known from other detector systems such as Timepix, have been found under continuous low flux irradiation. The integrated detector signal shows linear increase with particle fluence, estimating a saturation limit of 10^7 protons/cm^2 for 20 MeV protons, which is in good agreement with the quoted saturation limit of the detector [13].

To determine the single proton response of the sensor, the device was irradiated with a 15 MeV proton beam with a flux of about 10^4 protons/cm^2/s. The low flux ensured that the majority of pixel hits is associated with single protons and hence, allowed to investigate if charge sharing effects between neighbor pixels occur. For 75% of all detected events only single pixel responded. In case of two or more simultaneously responding neighbor pixels, so-called pixel clusters, pixel values of all responding pixels were summed to yield a single response signal (cluster sum). In presence of charge sharing the cluster sum is expected to yield a similar value as the pixel value of a single responding pixel. However, all analyzed clusters did not only show significantly higher cluster sum values as expected, but the cluster sum also scaled with the associated number of pixels in a cluster. Corresponding pixel value spectra of the cluster pixels were similar to the pixel value spectrum of single pixel hits. Hence, pixel clusters are not related to charge sharing effects but have to be attributed to simultaneous proton hits in adjacent pixels [13]. Figure 1 shows the pixel value spectrum of all hit pixels. Pixel values are measured in ADU (Analog-to-Digital Unit). Two peaks, corresponding to single and double proton hits per pixel can be distinguished. The distribution is fit by the sum of two Landau distributions to determine the most probable pixel values for single and double hits, respectively. Values for the corresponding energy loss within a sensitive detector thickness of 2 μm, according to the approximate pixel capacitance of 15 pF, are obtained from a TRIM simulation [22]. The thickness of the passivation layer, assumed to be 2 μm [23], as well as beam exit window are considered in the simulation. Using the single and double proton hit data,

2013 JINST 8 P03008

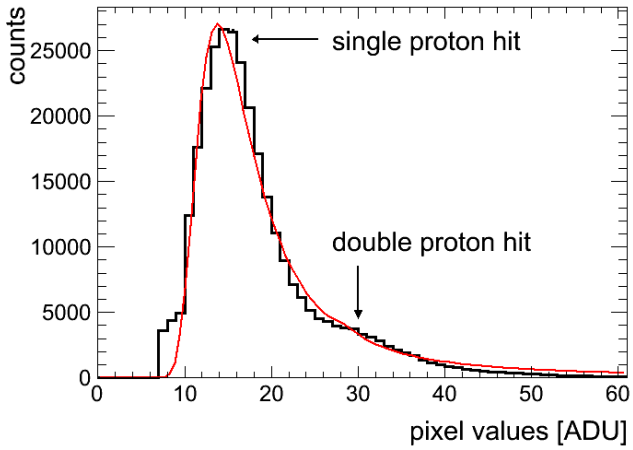

Figure 1. Background-corrected pixel value distribution measured in a mono-energetic, low flux proton beam of 15 MeV energy. Pixel values are measured in ADU, a unit related to the analog-to-digital conversion of the detector signal. The solid red line represents a fit by the sum of two Landau functions.

an energy loss to pixel value conversion factor of 1.09 ± 0.12 ADU/keV is obtained by a linear fit through the origin and both data points. The uncertainty of the conversion factor is associated with the fit uncertainty.

3.2 Radiation hardness

To investigate the sensors radiation hardness damage studies have been accomplished with protons as well as C-ions. The increase of the average dark pixel value was analyzed immediately after exposure in a small ROI of 20 (30) pixel diameter in case of proton (C-ion) irradiations. The result of the proton damage analysis is depicted in figure 2, where the average dark pixel value is plotted against proton fluence, showing a strong exponential increase with fluence. No dead pixels are observed even for the maximum fluence of $6 \cdot 10^{10}$ protons/cm^2. A similar trend with fluence is observed for the carbon data, although the average dark pixel value saturates for all fluences exceeding 10^{10} C-ions/cm^2, which were, therefore, not included in the analysis. Nevertheless, the detector is fully operational in undamaged regions above and below areas that have been exposed to the highest carbon fluence of 10^{12} particles/cm^2 while some charge overflow is visible in neighbour pixels lying in the direction of the sensor read-out. The ratio of proton to carbon fluence that yields the same dark pixel value increase is consistent with the ratio of corresponding energy loss values, obtained from SRIM [21].

The dynamic range loss that is associated with the increased dark pixel value can limit the usefulness of the detector for the detection of laser accelerated proton pulses. The sensor shows similar response to pulses with up to 10^5 protons/cm^2/ns in areas with pre-damage levels of $1 \cdot 10^{10}$ and $6 \cdot 10^{10}$, corresponding to residual dynamic ranges of 97% and 50%, compared to an initially undamaged region (figure 3).

2013 JINST 8 P03008

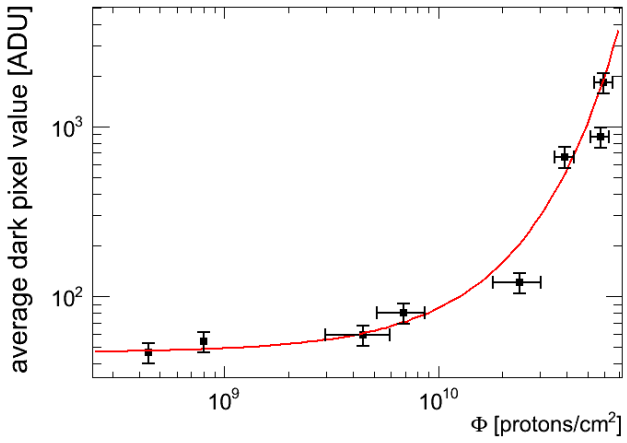

Figure 2. Pixel values of the unexposed sensor (dark pixel values) are a measure of the leakage current, which strongly depends on the total particle fluence on the detector. The solid red line represents an exponential fit of the data.

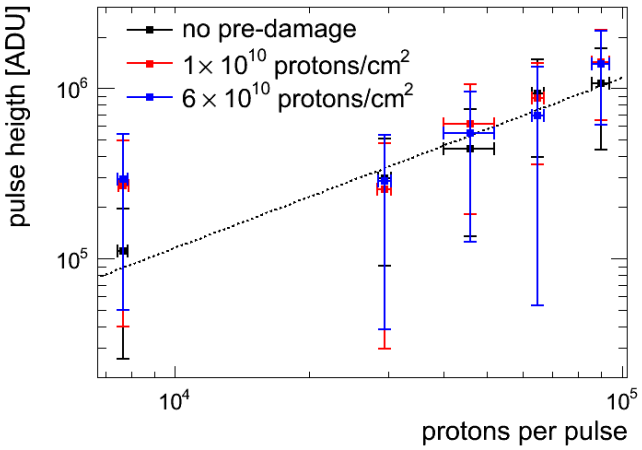

Figure 3. The pulse height, which corresponds to the integrated pixel value of all pixels hit by a single proton pulse, increases linearly with the pulse intensity. Even for the highest damage level of $6 \cdot 10^{10}$ p/cm^2, resulting in a dynamic range loss of 50%, no considerable difference in pulse response can be determined with respect to an undamaged device.

3.3 CR39 cross-calibration

A cross-calibration measurement with CR39 for low proton energies in the 1–3 MeV range was performed in a laser-accelerated proton beam. The Al foil, employed as filter for C-ions and light, introduces a cut-off of the proton spectrum in the low-energy region, corresponding to an energy of 1 MeV, which was used to establish the relationship between spatial detector and spectrometer (energy) coordinate that is required for data analysis. Corresponding energy ranges of 0.4 MeV

2013 JINST 8 P03008

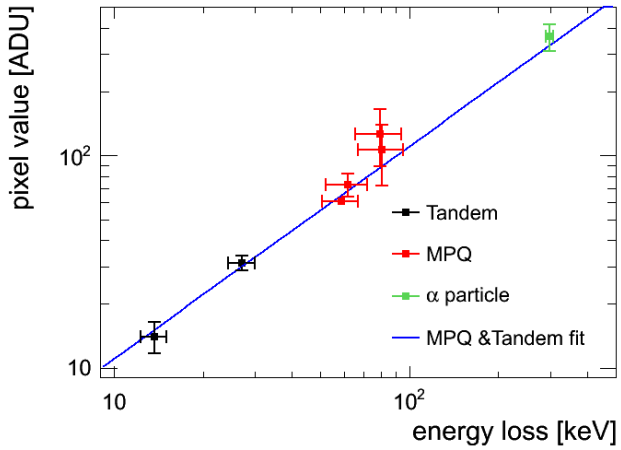

Figure 4. The detector response depends linearly on the energy loss within the sensitive layer, which was obtained by a TRIM simulation. The solid blue line represents a linear fit, including Tandem as well as MPQ measurements. Extrapolation of the fit curve to even higher values of the energy loss is possible, shown by the good agreement with an α-measurement.

width and average energies of about 1.5 MeV and 2.0 MeV, respectively, were analyzed on CR39 as well as the pixel detector. All pixel values within such energy regions have been summed and divided by the average proton number obtained from CR39 in corresponding energy region to determine the average single proton response of the sensor. Figure 4 shows the resulting calibration, plotting pixel values against energy loss. The single and double proton response values from the Tandem measurement are also included. Data of the Tandem and ATLAS calibration agree with each other. A linear fit through the origin and both data sets yields a single energy loss to pixel value conversion factor of (1.11 ± 0.09) ADU/keV. This energy calibration was cross-checked with a mixed nuclide α-source (239Pu, 241Am, 244Cm). The energy resolution of the detector is not sufficient to resolve individual α-lines in the spectrum. However, using an average energy loss for all three lines, the extrapolation of the calibration curve to higher energies is in good agreement with the α irradiation.

3.4 Measurements at the Astra-Gemini laser

The setup at the Astra-Gemini laser allowed simultaneous detection of protons and carbon ions with the calibrated pixel detector system. C-ions are mainly distributed within the charge state 6+. Using the energy loss calibration obtained from the Tandem and Atlas calibration, ion numbers per solid angle and energy were obtained from the measured proton and $^{6+}$C traces (small inset in figures 5, 6). This particular shot produced maximum energies of 10 MeV and 47 MeV for proton and ^{6}+C (5, 6). We estimated the accuracy in particle number determination to 10%. Although a background correction was accomplished before data analysis, single pixels in the background region show elevated signal levels. The origin of these hits is not yet fully understood and topic of further investigations.

2013 JINST 8 P03008

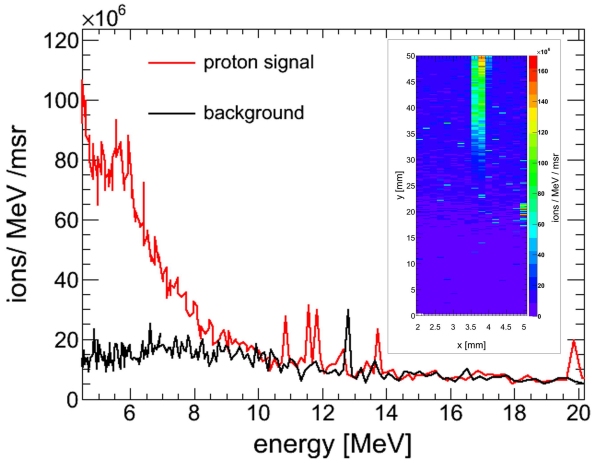

Figure 5. Proton signal and background level can not be distinguished for proton energies exceeding 10 MeV, thus defining the maximum cut-off energy. The small inset shows the 2D image of the proton trace. Proton energy decreases with increasing y-values. It can be clearly seen that the noise floor decreases with energy. Further investigations are required to understand this behavior.

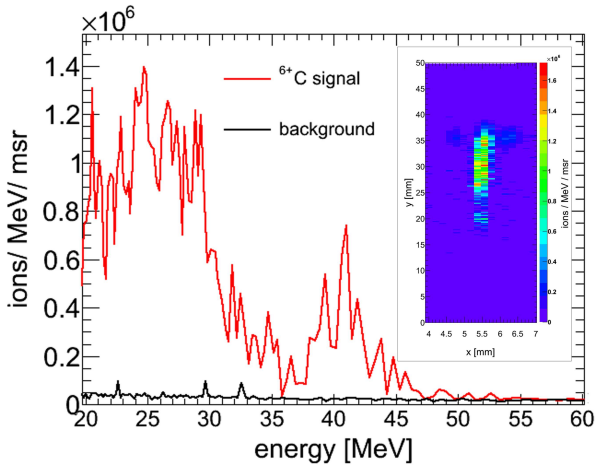

Figure 6. The ^{6}+C signal is clearly separated from the background level. The small inset shows the 2D distribution measured by the pixel detector. Raw sensor data (ADU values) have been converted into particle number/MeV/msr using the energy calibration from Tandem and ATLAS measurements. Almost circularly shaped elevated noise levels on each side of the trace are attributed to radiation damage.

4 Discussion

The dynamic range requirements of any (electronic) detector used behind a spectrometer are defined by the laser-accelerated ion spectrum. The low-energy part of the spectrum is usually characterized by a large particle number which goes down to single particles in the high-energy tail. The detector system, therefore, requires a large dynamic range and, ideally, also offers single ion sensitivity. Single ion detection was possible for all investigated energies up to 20 MeV. A limitation on the maximum energy for unambiguous single ion sensitivity is set by typical noise fluctuations of

2013 JINST 8 P03008

about 7 ADU. Extrapolation of the energy calibration yields a value for the energy deposition that corresponds to a proton energy of 35 MeV. The dynamic range of the investigated systems spans more than six orders of magnitude from single protons to pulses of more than 10^6 protons/cm^2/ns with respect to a proton energy of 20 MeV. The thin depletion layer, typical for such a device that is optimized for visible light detection, is an advantage with respect to the saturation level although limiting its usefulness for spectroscopic applications, as was seen by the measurement with the mixed α-source. However, if the energy of an incident particle is known, single particle discrimination is possible on a per pixel base.

Any silicon-based detector is damaged by incident ionizing radiation, in particular for particles with high stopping power, such as heavy ions or low-energy protons. An increase in the dark pixel value is observed even at low irradiation doses long before any electrical break down of the device. The dark pixel value shows an exponential increase with fluence for proton as well as C-ions. The amount of the leakage current increase depends on the total deposited dose and is independent on particle type. This is also confirmed by a damage study accomplished by the manufacturer with X-rays, where similar dose levels as in case of our radiations yield similar values of the dark current increase [23]. The observed exponential increase of the leakage current indicates that bulk damage in the silicon, associated with displacement damage, is not the dominant damage mechanism for this kind of active pixel sensor (APS). Each of the detector pixels incorporates three MOSFETs, that form a source follower. The main damaging mechanism is, therefore, related to positive charge build-up in the oxide layer of the transistors, changing the charge carrier density in the depletion region which leads to an increase in dark current [23]. After a radiation dose of about 100 Gy the dynamic range decreased by a factor of 2. Nevertheless, a linear response to proton pulse fluences up to 10^5 protons/cm^2 was observed even for this damage level. No significant response difference between damaged and undamaged areas has been found in a comparison of areas with different pre-damage levels. For the detection of laser-accelerated ions the dynamic range of the detector is an important parameter. In the following, the term detector lifetime is referred to a maximum tolerable dynamic range reduction for this kind of application and not associated with any electrical break down of the device. The need to replace the detector is triggered by the minimum tolerable dynamic range which is associated with a total dose. For instance, considering single pulses containing 10^7 protons/cm^2 of 20 MeV energy and a tolerable dynamic range reduction of only 10%, about 3000 pulses can be detected before replacement is required. The total pulse number scales with the single shot dose and, therefore, primarily LET (linear energy transfer) of the incident particles. Maximum proton energies of 58 MeV have been reported in the past [24], with further increasing particle energies the lifetime issue will relax. However, as the most interesting part of the laser-accelerated ion spectrum is usually the high-energy tail it can be beneficial to block contributions of the low-energy particles (e.g. with energy < 1 MeV/u) with respect to the detector's replacement rate. This approach was used in the CR39 cross-calibration at the Atlas laser to block all contributions from C-ions and low-energy protons by means of a thin Aluminium foil. No disturbance of the detector response related to EMP emission during laser-target interaction was observed in these measurements. This was also confirmed by recent measurements at the DRACO laser and Astra-Gemini Laser. The cross-calibration with CR39 showed an excellent agreement with the calibration obtained at the Tandem accelerator. The measurement with the α-source showed good agreement with the extrapolated fit of the energy loss calibration. Although calibration data were obtained

2013 JINST 8 P03008

by proton irradiations, the relationship between energy loss and detector response is independent on particle type and even more important linear overt the whole dynamic range of the detector unlike 'organic' detectors such as RCF or scintillators. Used behind a spectrometer, spatial detector coordinates are related to the energy of incident particles. The detector calibration can be used to determine the number of particles within an energy range. The energy deposition within the sensitive layer has to be obtained from a simulation. The feasibility of this approach was demonstrated in an experiment at the Astra-Gemini Laser. Proton and $^{6+}$C-ions were simultaneously detected on the sensor. Using the energy calibration obtained in experiments at the Tandem and Atlas laser and appropriate energy loss simulations for both ion species, the particle number per energy bin and solid angle could be determined. Maximum cut-off energies are visible in both spectra. The accuracy of the simulation and, hence, particle number determination depends on a precise mapping of detector coordinate and spectrometer coordinate. The feasible energy resolution, which is theoretically only determined by both, spectrometer resolution and spatial resolution of the pixel detector also depends on the accuracy of the established coordinate relationship. Assuming a negligible energy spread on a per-pixel base, the uncertainty of the conversion factor determines a lower limit for the accuracy in particle number determination of about 8%.

A directly competing detector system for the detection of laser-accelerated ion spectra behind a spectrometer are MCPs coupled to a phosphor screen whose light output is detected by a CCD camera [9–11, 25]. The single ion sensitivity of a MCP-based detector system depends on the secondary electron emission (SEM) probability which scales with the energy loss of incident particles. For a proton with an energy in the MeV range, the emission probability is in the order of only few percent. To determine the total detection efficiency of such a combined diagnostic system, collection efficiencies of the camera lens, the quantum efficiency of the CCD camera at the phosphor emission wavelength and sensitive area of the MCP have also to be considered. A detection efficiency of only 0.7% has, thus, been reported for a proton energy of 13 MeV which increases to about 10% for 2 MeV for a typical MCP-based system [25]. The typical dead time of a single MCP channel of 10 ms when operated in pulsed mode, exceeds the duration of a laser-accelerated ion pulse by several orders of magnitude. Assuming a SEM probability of 1, the number of MCP channels per cm^2 corresponds to the maximum detectable particle fluence, which is 10^6/cm^2 for typical channel diameters of 10 μm.

The response of both diagnostic systems changes with increasing radiation dose. Minimum dynamic range requirements usually limit the time period that such a device can be used for quantitative detection before complete device break down occurs. For the MCP-based system performance changes are associated with a degradation in gain. For instance, an accumulated charge of about 0.1 C/cm^2 after electron irradiation yields a gain reduction of 20% in case of an MCP [12]. The accumulated charge corresponds to a proton fluence of $6 \cdot 10^{10}$, assuming single electron generation per incident proton and an initial gain of 10^7. A similar proton number, referring to a proton energy of 20 MeV, reduces the dynamic range in case of the pixel detector by 50%. Although the MCP-based system is more robust with respect to radiation hardness, the lifetime of the pixel detector is still sufficient for the planned application. As the approach is based on a commercial sensor, produced in large quantities at reasonable costs, replacement is possible. The high voltage that is required for MCP operation demands a good vacuum of better 10^{-6} mbar. In contrast, the pixel detector can be operated in vacuum as well as air, which simplifies the experimental setup considerably.

2013 JINST 8 P03008

5 Conclusion

We demonstrated a compact, large-area pixel detector system that can be applied behind a spectrometer as an online detector for laser-accelerated ions. Careful calibrations showed neither dose rate dependence nor EMP sensitivity in laser-acceleration experiments, so far. The pulse dose response is linear over the whole dynamic range of the device.

The pixel detector system is also able to compete with MCP-based detection systems that are also used behind a spectrometer for measurement of laser-accelerated ion spectra. The saturation levels of both detector types are comparable for few MeV proton energies. The considerably higher single particle sensitivity of the pixel detector is as an advantage compared to the MCP-based system. The pixel detector system combines computer and read-out electronics in a simple setup, which is in addition to the ease of use and little demands on experimental conditions a particular benefit by contrast with MCP operational requirements. The pixel detector system has shown to be a mature system for laser-ion diagnostics for the present state of laser-ion-acceleration.

Acknowledgments

The authors would like to thank Klaus Allinger, Jianhui Bin, Peter Hilz and Wenjun Ma of the laser ion acceleration group at the MPQ Atlas Laser for operation of the laser accelerator. Supported by the DFG Cluster of Excellence: Munich Centre for Advanced Photonics (MAP).

References

[1] V. Malka, J. Faure, Y.A. Gauduel, E. Lefebvre, A. Rousse and K.T. Phuoc, *Principles and applications of compact laser-plasma accelerators*, *Nature Phys.* **4** (2008) 447.

[2] H. Daido, M. Nishiuchi and A.S. Pirozhkov, *Review of laser-driven ion sources and their applications*, *Rep. Prog. Phys.* **75** (2012) 056401.

[3] V.T. Tikhonchuk, *Physics of laser-assisted ion acceleration*, *Nucl. Instrum. Meth.* **A 620** (2010) 1.

[4] I.W. Choi et al., *Absolute calibration of a time-of-flight spectrometer and imaging plate for the characterization of laser-accelerated protons*, *Meas. Sci. Technol.* **20** (2009) 115112.

[5] S. Gaillard, J. Fuchs, N. Renard-Le Galloudec and T.E. Cowan, *Study of saturation of CR39 nuclear track detectors at high ion fluence and of associated artifact patterns*, *Rev. Sci. Instrum.* **78** (2007) 013304.

[6] D.S. Hey et al., *Use of GafChromic film to diagnose laser generated proton beams*, *Rev. Sci. Instrum.* **79** (2008) 053501.

[7] D. Kirby et al., *Radiochromic film spectroscopy of laser-accelerated proton beams using the FLU.K.A code and dosimetry traceable to primary standards*, *Laser Part. Beams* **29** (2011) 231.

[8] A. Mancic, J. Fuchs, P. Antici, S.A. Gaillard and P. Audebert, *Absolute calibration of photostimulable image plate detectors used as (0.5–20 MeV) high-energy proton detectors*, *Rev. Sci. Instrum.* **79** (2008) 073301.

[9] K. Harres et al., *Development and calibration of a Thomson parabola with microchannel plate for the detection of laser-accelerated MeV ions*, *Rev. Sci. Instrum.* **79** (2008) 093306.

2013 JINST 8 P03008

[10] R. Prasad et al., *Calibration of Thomson parabola-MCP assembly for multi-MeV ion spectroscopy*, *Nucl. Instrum. Meth.* **A 623** (2010) 712.

[11] S. Ter-Avetisyan, L. Romagnani, M. Borghesi, M. Schnurer and P.V. Nickles, *Ion diagnostics for laser plasma experiments*, *Nucl. Instrum. Meth.* **A 623** (2010) 709.

[12] J.L. Wiza, *Microchannel Plate Detectors*, *Nucl. Instrum. Meth.* **162** (1979) 587.

[13] S. Reinhardt, C. Granja, F. Krejci and W. Assmann, *Test of pixel detectors for laser-driven accelerated particle beams*, 2011 *JINST* **6** C12030.

[14] Rad-icon Imaging Corporation, *RadEye™1 Large area Image Sensor*, http://www.rad-icon.com.

[15] T. Graeve and G.P. Weckler, *High-resolution CMOS imaging detector*, http://www.rad-icon.com.

[16] T. Graeve and G.P. Weckler, *Large Area Digital X-ray Specific Imager*, http://www.rad-icon.com.

[17] M. Moser et al., *High brilliance multicusp ion source for hydrogen microscopy at SNAKE*, *Nucl. Instrum. Meth.* **B 273** (2012) 226.

[18] W.J. Ma et al., *Preparation of self-supporting diamond-like carbon nanofoils with thickness less than 5 nm for laser-driven ion acceleration*, *Nucl. Instrum. Meth.* **A 655** (2011) 53.

[19] G. Rusch, E. Winkel, A. Noll and W. Heinrich, *The Siegen Automatic Measuring System for Track Detectors — New Developments*, *Nucl. Tracks Radiat. Meas.* **19** (1991) 261.

[20] W. Trakowski et al., *An Automatic Measuring System for Particle Tracks in Plastic Detectors*, *Nucl. Instrum. Meth.* **A 225** (1984) 92.

[21] J.F. Ziegler, M.D. Ziegler and J.P. Biersack, *SRIM — The stopping and range of ions in matter*, *Nucl. Instrum. Meth.* **B 268** (2010) 1818.

[22] R. Schmid-Fabian, private communication (2011).

[23] Rad-icon Imaging Corporation, *Detector Lifetime and Radiation Damage*, http://www.rad-icon.com.

[24] R.A. Snavely et al., *Intense high-energy proton beams from petawatt-laser irradiation of solids*, *Phys. Rev. Lett.* **85** (2000) 2945.

[25] W. Mroz et al., *Thomson parabola ion spectrograph with the microchannel plate image converter in investigations of high-Z laser plasma ion sources*, *Rev. Sci. Instrum.* **67** (1996) 1272.

2013 JINST 8 P03008